J Braz. Soc. Mech. Sci. Eng. (2017) 39:3005–3017
DOI 10.1007/s40430-017-0743-7

TECHNICAL PAPER

Mixed convective stagnation point flow of Carreau fluid with variable properties

M. Waqas[1] · A. Alsaedi[2] · S. A. Shehzad[3] · T. Hayat[1,2] · S. Asghar[4]

Received: 21 April 2015 / Accepted: 22 February 2017 / Published online: 17 March 2017

Abstract Here, our aim is to address the mixed convective stagnation point flow of Carreau liquid over a moving permeable surface. Constitutive expression of an incompressible Carreau liquid is taken into account. The assumptions of boundary layer are implemented in the mathematical modeling of considered physical phenomenon. A well-known analytical technique homotopy analysis method is employed for the computations of governing equations. The numerical data of skin friction coefficient and local Nusselt number is obtained and explored. The velocity is enhanced for larger ratio of rate constants. The increasing values of suction parameter correspond to less velocity and temperature profiles. Further, a benchmark is presented to validate the solutions obtained here. It is noted that the computed analytical solutions have excellent match with previous published materials in a limiting manner.

Keywords Mixed convection · Stagnation point flow · Carreau fluid · Variable properties

Technical Editor: Cezar Negrao.

✉ S. A. Shehzad
ali_qau70@yahoo.com

1 Department of Mathematics, Quaid-I-Azam University, 45320, Islamabad 44000, Pakistan

2 Nonlinear Analysis and Applied Mathematics (NAAM) Research Group, Department of Mathematics, Faculty of Science, King Abdulaziz University, Jeddah 21589, Saudi Arabia

3 Department of Mathematics, COMSATS Institute of Information Technology, Sahiwal 57000, Pakistan

4 Department of Mathematics, COMSATS Institute of Information Technology, Chak Shehzad, Park Road, Islamabad 44000, Pakistan

1 Introduction

Nowadays, the dynamics of non-Newtonian liquids is a subject of abundant researches for the scientists and engineers due to its practical implementation. The technological and industrial applications of such liquids include molten polymers, drilling muds, volcanic lava, oils, certain paints, liquid suspensions, cosmetic products, poly crystal melts, food stuffs and many more. The flow phenomenon of such materials can be elaborated by the nonlinear relationships of shear rate and shear stresses. The viscosity of such liquids is shear dependent. The Carreau liquid model is one of the non-Newtonian liquid models which have the constitutive relationship for both high and low shear rates. This fact enhanced the utilization of Carreau model in technological and industrial processes. Hsu et al. [1] developed a model to describe the importance of electrophoresis on Carreau liquid in a spherical cavity. Peristaltic motion in an asymmetric channel filled with Carreau fluid has been addressed by Ali and Hayat [2]. Shamekhi and Sadeghy [3] explored characteristics of Carreau-Yasuda liquid in a cavity by employing PIM mesh-free method. The flow phenomenon of Carreau fluid over an inclined free surface has been reported by Tshehla [4]. Olajuwon [5] described the analysis convective heat and mass transport in magnetohydrodynamic flow of Carreau liquid induced by a porous plat. He also examined the thermal diffusion and radiation effects in this study. The boundary layer flow analysis of Carreau liquid due to a convectively heated sheet has been made by Hayat et al. [6]. Magnetohydrodynamic (MHD) Falkner-Skan wedge flow of Carreau liquid with cross-diffusion effects is presented by Raju and Sandeep [7]. Machireddy and Naramgari [8] examined the characteristics of cross-diffusion in MHD flow of Carreau liquid over a stretched surface with Robin boundary condition. Stagnation point flow of Carreau nanofluid with transpiration is explored by Sulochana et al. [9]. Raju and Sandeep [10] studied the three-dimensional (3D) flow of Casson-Carreau fluids over a stretched surface subject to homogeneous/heterogeneous reactions and nonlinear thermal radiation. Hayat et al. [11] explored the stretching flow phenomenon of Carreau nanoliquid.

The stagnation point flow arises whenever a flow imposes on a solid object. The motion of liquid near stagnation region is described by stagnation point flow which exists for both cases of moving or fixed body in a liquid. Hiemenz [12] firstly explored the phenomenon of stagnation point flow over a stationary semi-infinite wall. He demonstrated that the Navier–Stokes expressions which govern the flow can be converted into ordinary differential equations by the utilization of similarity transformation. Mahaputra and Gupta [13] studied the heat transport analysis of stagnation point flow over a moving sheet. Nazar et al. [14] studied the flow of micropolar fluid over a stretched sheet. Mustafa et al. [15] studied the stagnation point flow of a nanofluid towards a stretching surface. Alsaedi et al. [16] achieved the results for the effects of heat sink/source of nanofluid near a stagnation point over a surface with convective conditions. Turkyilmazoglu and Pop [17] investigated the boundary layer flow of Jeffrey fluid near a stagnation point over a shrinking/stretching sheet. Hayat et al. [18] addressed the stagnation point flow of second grade liquid. Shehzad et al. [19] reported the effect of chemical reaction in steady stagnation point flow of thixotropic liquid.

The aim of this investigation is to make an analysis of mixed convective stagnation point flow of Carreau liquid over a stretched sheet. The governing mathematical expressions are coupled due to occurrence of mixed convection. Analytical solutions via homotopy analysis method (HAM) [20–29] are constructed. Relevant convergence criteria of solutions is established and examined. Plots of various quantities are elaborated and discussed.

2 Mathematical formulation

Here, we consider the two-dimensional steady mixed convection flow of an incompressible Carreau liquid towards a stretched surface near a stagnation point. The sheet is stretched in such a manner that x-axis is along the surface of sheet and y-axis perpendicular to it. An incompressible fluid flow is confined to $y > 0$. The thermo-physical characteristics of liquid at surface are taken variable. The constitutive relation for Carreau material is [6]:

$$\boldsymbol{\tau} = \left[\eta_0\left(1+\lambda^2\dot{\gamma}^2\right)^{\frac{n-1}{2}}\right]\mathbf{A}_1, \tag{1}$$

where

$$\mathbf{A}_1 = \nabla\mathbf{V}+(\nabla\mathbf{V})^{tr}, \tag{2}$$

$$\dot{\gamma} = \sqrt{\frac{1}{2}tr(\mathbf{A}_1)^2}, \tag{3}$$

$$\mathbf{V} = \left[u(x,y),\, v(x,y),\, 0\right], \tag{4}$$

$$\dot{\gamma}^2 = 2\left(\frac{\partial u}{\partial x}\right)^2 + 2\left(\frac{\partial v}{\partial y}\right)^2 + \left(\frac{\partial u}{\partial y}+\frac{\partial v}{\partial x}\right)^2, \tag{5}$$

or

$$\dot{\gamma}^2 = 4\left(\frac{\partial u}{\partial x}\right)^2 + \left(\frac{\partial u}{\partial y}+\frac{\partial v}{\partial x}\right)^2. \tag{6}$$

Now

$$\tau = \eta_0\left[1+\lambda^2\left\{4\left(\frac{\partial u}{\partial x}\right)^2 + \left(\frac{\partial u}{\partial y}+\frac{\partial v}{\partial x}\right)^2\right\}\right]^{\frac{n-1}{2}}\mathbf{A}_1, \tag{7}$$

with

$$\boldsymbol{\tau}_{xx} = 2\eta_0\left[1+\lambda^2\left\{4\left(\frac{\partial u}{\partial x}\right)^2 + \left(\frac{\partial u}{\partial y}+\frac{\partial v}{\partial x}\right)^2\right\}\right]^{\frac{n-1}{2}}\frac{\partial u}{\partial x}, \tag{8}$$

$$\boldsymbol{\tau}_{xy} = \eta_0\left[1+\lambda^2\left\{4\left(\frac{\partial u}{\partial x}\right)^2 + \left(\frac{\partial u}{\partial y}+\frac{\partial v}{\partial x}\right)^2\right\}\right]^{\frac{n-1}{2}}\left(\frac{\partial u}{\partial y}+\frac{\partial v}{\partial x}\right) = \boldsymbol{\tau}_{yx}, \tag{9}$$

$$\boldsymbol{\tau}_{yy} = 2\eta_0\left[1+\lambda^2\left\{4\left(\frac{\partial u}{\partial x}\right)^2 + \left(\frac{\partial u}{\partial y}+\frac{\partial v}{\partial x}\right)^2\right\}\right]^{\frac{n-1}{2}}\frac{\partial v}{\partial y}. \tag{10}$$

Since

$$\rho(\nabla.\mathbf{V}) = \nabla.\tau, \tag{11}$$

so inserting Eqs. (4), (8) and (9) in Eq. (11) we obtain

$$u\frac{\partial u}{\partial x} + v\frac{\partial u}{\partial y} = \nu\frac{\partial^2 u}{\partial y^2}\left[1+\left(\frac{n-1}{2}\right)\lambda^2\left(\frac{\partial u}{\partial y}\right)^2\right]$$

$$+\nu(n-1)\lambda^2\left(\frac{\partial^2 u}{\partial y^2}\left(\frac{\partial u}{\partial y}\right)^2\right)\left(1+\left(\frac{n-3}{2}\right)\lambda^2\left(\frac{\partial u}{\partial y}\right)^2\right). \tag{12}$$

Two-dimensional flow equations for Carreau liquid in the presence of stagnation point, variable viscosity, mixed convection, thermal radiation and temperature-dependent thermal conductivity are:

$$\frac{\partial u}{\partial x}+\frac{\partial v}{\partial y}=0, \tag{13}$$

$$u\frac{\partial u}{\partial x}+v\frac{\partial u}{\partial y}=\frac{1}{\rho}\frac{\partial}{\partial y}\left(\eta_0(T)\frac{\partial u}{\partial y}\right)+v\frac{\partial^2 u}{\partial y^2}\left[1+\left(\frac{n-1}{2}\right)\lambda^2\left(\frac{\partial u}{\partial y}\right)^2\right]$$
$$+(n-1)\lambda^2\left[\frac{\partial^2 u}{\partial y^2}\left(\frac{\partial u}{\partial y}\right)^2\right]\left[1+\left(\frac{n-3}{2}\right)\lambda^2\left(\frac{\partial u}{\partial y}\right)^2\right]$$
$$+u_e\frac{\mathrm{d}u_e}{\mathrm{d}x}+g\beta_T(T-T_\infty), \tag{14}$$

$$u\frac{\partial T}{\partial x}+v\frac{\partial T}{\partial y}=\frac{1}{\rho c_p}\frac{\partial}{\partial y}\left(K(T)\frac{\partial T}{\partial y}\right)+\frac{16\sigma^*}{3k^*\rho c_p}\frac{\partial}{\partial y}\left(T^3\frac{\partial T}{\partial y}\right), \tag{15}$$

$$u=u_w(x)=cx,\quad v=v_w,\quad T=T_w(x)=T_\infty+bx\quad \text{at}\quad y=0,$$
$$u\to u_e(x)=ax,\quad T\to T_\infty\quad \text{as}\quad y\to\infty. \tag{16}$$

In the above equations, u and v denote the velocity components in the x and y-directions, respectively, λ the time constant, T the fluid temperature, ν the kinematic viscosity, ρ the density, c_p the specific heat, $\eta_0(\mathrm{T})$ the variable dynamic viscosity depending on temperature, g the gravitational acceleration, β_T the thermal expansion coefficient, the σ^* Steafan-Boltzmann constant, k^* the mean absorption coefficient, (a, b, c) the dimensional constants, v_w is the mass transfer velocity and T_w the variable temperature at the sheet and T_∞ the ambient temperature. The constant mass transfer velocity is taken as v_w. Here $v_\mathrm{w}>0$ denotes injection or blowing, $v_\mathrm{w}<0$ for suction and u_e the free stream velocity.

Thermal conductivity $K(T)$ and variable viscosity $\eta_0(T)$ are [30, 31]:

$$K(T)=k_\infty\left(1+\varepsilon\frac{T-T_\infty}{\Delta T}\right), \tag{17}$$

$$\frac{1}{\eta_0(T)}=\frac{1}{\eta_\infty}\left[1+\gamma(T-T_\infty)\right], \tag{18}$$

or

$$\frac{1}{\eta_0(T)}=\delta(T-T_r), \tag{19}$$

where

$$\delta=\frac{\gamma}{\eta_\infty}\quad\text{and}\quad T_\mathrm{r}=T_\infty-\frac{1}{\gamma}, \tag{20}$$

here k_∞ is the thermal conductivity of the ambient fluid, ε is a small scalar parameter which portrays the impact of temperature on variable thermal conductivity, $\Delta T=T_\mathrm{w}-T_\infty$, η_∞ the ambient dynamic viscosity, γ the thermal property of fluid, (δ, T_r) are the constants and their values depend upon the thermal state and thermal property, i.e., γ. Also $\delta>0$ for liquids and $\delta<0$ for gases.

To transform the above problem in dimensionless form, we employ

$$\eta=y\sqrt{\frac{c}{\nu}},\quad u=cxf'(\eta),\quad v=-\sqrt{c\nu}f'(\eta),\quad \theta(\eta)=\frac{T-T_\infty}{T_\mathrm{w}-T_\infty}. \tag{21}$$

The continuity Eq. (13) is identically satisfied, and the resulting problems in f and θ are reduced to the following forms

$$f'''\left[1+\left(\frac{n-1}{2}\right)\lambda_1 f''^2\right)+2\left(\left(\frac{n-1}{2}\right)\lambda_1 f''^2\right)\left(1+\left(\frac{n-3}{2}\right)\lambda_1 f''^2\right]$$
$$+\left(\frac{\theta'}{\theta_r-\theta}\right)f''+\left(\frac{\theta_r-\theta}{\theta_r}\right)\left(ff''-f'^2+G\theta+A^2\right)=0, \tag{22}$$

$$\left(1+\frac{4}{3}N+\varepsilon\theta\right)\theta''+\varepsilon\theta'^2+\Pr\left(f\theta'-f'\theta\right)=0, \tag{23}$$

$$f=S,\quad f'=1,\quad \theta=1\quad\text{at}\quad\eta=0,$$
$$f'=A,\quad \theta=0\quad\text{as}\quad\eta\to\infty, \tag{24}$$

where prime signifies differentiation with respect to η and dimensionless quantities can be expressed as follows:

$$\lambda_1=\lambda^2c^2,\quad S=-\frac{v_\mathrm{w}}{\sqrt{c\nu}},\quad \Pr=\frac{\nu}{\alpha},$$
$$\theta_\mathrm{r}=\frac{T_\mathrm{r}-T_\infty}{T_\mathrm{w}-T_\infty}=-\frac{\eta_\infty}{\gamma(T_\mathrm{w}-T_\infty)},\quad G=\frac{Gr_x}{Re_x^2}=\frac{g\beta_T b}{c^2},$$
$$Gr_x=\frac{g\beta_\mathrm{T}(T_\mathrm{w}-T_\infty)x^3}{\nu^2},$$
$$Re_x=\frac{u_\mathrm{w}(x)x}{\nu},\quad A=\frac{a}{c},\quad N=\frac{4\sigma^*T_\infty^3}{k^*K(T)}. \tag{25}$$

Here, λ_1 denotes the material parameter, S the mass transfer parameter with $S>0$ for suction and $S<0$ for injection, Pr the Prandtl number, θ_r the variable viscosity parameter, G the mixed convection parameter, Gr_x the Grashof number, Re_x the Reynolds numbers, A the ratio of rate constants and N the thermal radiation parameter.

The terms $\left(1+\frac{4}{3}N\right)$ and Pr in Eq. (23) can be combined. In this way, a single parameter is obtained i.e. $\Pr_\mathrm{eff}=\frac{3\Pr}{3+4N}$. Hence Eq. (23) takes the form [32, 33]:

$$\theta''+\Pr_\mathrm{eff}\left(f\theta'-f'\theta\right)+\varepsilon\theta\theta''+\varepsilon\theta'^2=0, \tag{26}$$

in which $\Pr_{\mathrm{eff}}$ is known as the effective Prandtl number. Benefit of aforementioned combination is that effects of linear radiation are neglected and the problem reduces to the case of without radiation. Idea of such combination can be found in the analysis provided in [32, 33].

The skin friction coefficient C_{f} and local Nusselt number Nu_{x} are defined as

$$C_{\mathrm{f}} = \frac{\tau_{\mathrm{w}}}{\frac{1}{2}\rho u_{\mathrm{w}}^2}, \quad Nu_{\mathrm{x}} = -\frac{x q_{\mathrm{w}}}{K(T)(T_{\mathrm{w}} - T_\infty)}, \tag{27}$$

where

$$\tau_{\mathrm{w}} = \eta_0(T)\left[\left(\frac{\partial u}{\partial y}\right) + \left(\frac{n-1}{2}\right)\lambda^2 \left\{ \begin{matrix} \frac{\partial u}{\partial y}\left(\frac{\partial u}{\partial x}\right)^2 + \\ 3\frac{\partial v}{\partial x}\left(\frac{\partial u}{\partial y}\right)^2 \end{matrix} \right\}\right]_{y=0},$$

$$q_{\mathrm{w}} = -\left(K(T) + \frac{16\sigma^* T_\infty^3}{3k^*}\right)\left(\frac{\partial T}{\partial y}\right)_{y=0}. \tag{28}$$

In terms of dimensionless form one has

$$\begin{gathered} C_f Re_x^{\frac{1}{2}} = \left(\frac{\theta_r}{\theta_r - 1}\right)\left(1 + \left(\frac{n-1}{2}\right)\lambda_1 \left(f'(0)\right)^2\right) \\ f''(0),\ Re_x^{-\frac{1}{2}} Nu_x = -\left(1 + \frac{4}{3}N\right)\theta'(0). \end{gathered} \tag{29}$$

3 Series solutions

The initial guesses and auxiliary linear operators are given below:

$$f_0(\eta) = A\eta + (1 - A)\left(1 - \mathrm{e}^{-\eta}\right), \quad \theta_0(\eta) = \mathrm{e}^{-\eta}, \tag{30}$$

$$L_{\mathrm{f}} = f''' - f', \quad L_\theta = \theta'' - \theta. \tag{31}$$

The above auxiliary linear operators satisfy the following properties

$$\begin{gathered} L_{\mathrm{f}}(C_1 + C_2\mathrm{e}^{\eta} + C_3\mathrm{e}^{-\eta}) = 0, \\ L_\theta(C_4\mathrm{e}^{\eta} + C_5\mathrm{e}^{-\eta}) = 0, \end{gathered} \tag{32}$$

where C_i $(i = 1$–$5)$ indicate the arbitrary constants.

The corresponding problems at the zeroth order are given in the following forms [22–24]:

$$(1-p)L_f\left[\hat{f}(\eta;\, p) - f_0(\eta)\right] = p\hbar_f \mathbf{N}_f\left[\hat{f}(\eta;\, p),\, \hat{\theta}(\eta,\, p)\right], \tag{33}$$

$$(1-p)L_\theta\left[\hat{\theta}(\eta;\, p) - \theta_0(\eta)\right] = p\hbar_\theta \mathbf{N}_\theta\left[\hat{f}(\eta;\, p),\, \hat{\theta}(\eta,\, p)\right], \tag{34}$$

$$\begin{gathered} \hat{f}(0;\, p) = 0, \quad \hat{f}'(0;\, p) = 1, \quad \hat{f}'(\infty;\, p) = A, \\ \hat{\theta}'(0,\, p) = 1, \quad \hat{\theta}(\infty,\, p) = 0, \end{gathered} \tag{35}$$

When $p = 0$ and $p = 1$ one has [25, 26]:

$$\begin{gathered} \hat{f}(\eta;\, 0) = f_0(\eta), \quad \hat{\theta}(\eta,\, 0) = \theta_0(\eta), \\ \hat{f}(\eta;\, 1) = f(\eta), \quad \hat{\theta}(\eta,\, 1) = \theta(\eta). \end{gathered} \tag{36}$$

Clearly when p is increased from 0 to 1 then $f(\eta, p)$ and $\theta(\eta, p)$ vary from $f_0(\eta)$, $\theta_0(\eta)$ to $f(\eta)$ and $\theta(\eta)$. By Taylor's expansion we have [27, 28]:

$$f(\eta,\, p) = f_0(\eta) + \sum_{m=1}^{\infty} f_m(\eta)p^m,\ f_m(\eta) = \frac{1}{m!}\frac{\partial^m f(\eta;\, p)}{\partial \eta^m}\bigg|_{p=0}, \tag{37}$$

$$\theta(\eta,\, p) = \theta_0(\eta) + \sum_{m=1}^{\infty} \theta_m(\eta)p^m,\ \theta_m(\eta) = \frac{1}{m!}\frac{\partial^m \theta(\eta;\, p)}{\partial \eta^m}\bigg|_{p=0}. \tag{38}$$

The convergence of above series strongly depends upon $\hbar_f$ and $\hbar_\theta$. Considering that $\hbar_f$ and $\hbar_\theta$ are selected properly so that Eqs. (37) and (38) converge at $p = 1$, then we can write

$$f(\eta) = f_0(\eta) + \sum_{m=1}^{\infty} f_m(\eta), \tag{39}$$

$$\theta(\eta) = \theta_0(\eta) + \sum_{m=1}^{\infty} \theta_m(\eta). \tag{40}$$

The resulting problems at mth order deformation can be constructed as follows:

$$L_f[f_m(\eta) - \chi_m f_{m-1}(\eta)] = \hbar_f \mathbf{R}_f^m(\eta), \tag{41}$$

$$L_\theta[\theta_m(\eta) - \chi_m \theta_{m-1}(\eta)] = \hbar_\theta \mathbf{R}_\theta^m(\eta), \tag{42}$$

$$f_m(0) = f_m'(0) = f_m'(\infty) = 0, \quad \theta_m(0) = \theta_m(\infty) = 0, \tag{43}$$

$$\begin{aligned} \mathbf{R}_f^m(\eta) = {} & f_{m-1}'''(\eta) + f_{m-1}''(\eta) + \frac{1}{\theta_r}\sum_{k=0}^{m-1} f_{m-1-k}''\theta_k \\ & - \frac{1}{\theta_r}\sum_{k=0}^{m-1}\sum_{l=0}^{k} \theta_{m-1-k}f_{k-l}f_l'' + \frac{1}{\theta_r}\sum_{k=0}^{m-1}\sum_{l=0}^{k} \theta_{m-1-k}f_{k-l}'f_l' \\ & + \lambda_1\left(\frac{n-1}{2}\right)\sum_{k=0}^{m-1}\sum_{l=0}^{k} f_{m-1-k}'''f_{k-l}''f_l'' + \sum_{k=0}^{m-1}\left[f_{m-1-k}f_k'' - f_{m-1-k}'f_k'\right] \\ & - \frac{1}{\theta_r}G\sum_{k=0}^{m-1}\theta_{m-1-k}\theta_k - \frac{1}{\theta_r}A^2\theta_{m-1} \\ & + 2\left(\frac{n-1}{2}\right)\lambda_1\sum_{k=0}^{m-1} f_{m-1-k}''f_k''\left[1 + \lambda_1\left(\frac{n-3}{2}\right)\sum_{l=0}^{k} f_{k-l}''f_l''\right] \\ & + (1-\chi_m)A^2 + \lambda\theta_{m-1} \end{aligned} \tag{44}$$

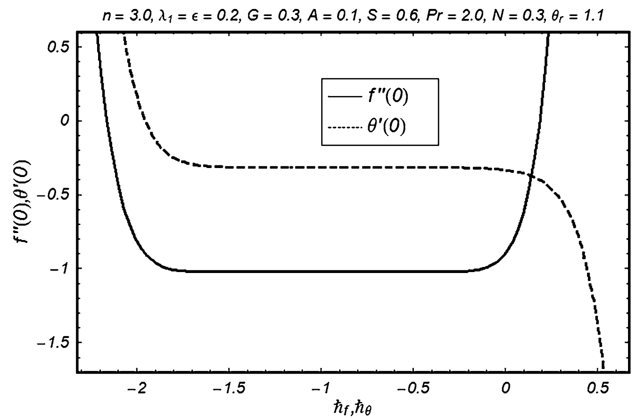

Fig. 1 $\hbar$-curve for f and θ

$$\mathbf{R}_m^{\theta}(\eta) = \left(1 + \frac{4}{3}N\right)\theta''_{m-1}(\eta) + \varepsilon\sum_{k=0}^{m-1}\theta_{m-1-k}\theta''_k + \varepsilon\sum_{k=0}^{m-1}\theta'_{m-1-k}\theta'_k + Pr_{eff}\sum_{k=0}^{m-1}\left(\theta'_{m-1-k}f_k - f'_{m-1-k}\theta_k\right), \quad (45)$$

Solving the above mth order deformation problems, the general solutions can be written as follows:

$$f_m(\eta) = f_m^*(\eta) + C_1 + C_2e^{\eta} + C_3e^{-\eta}, \quad (46)$$

$$\theta_m(\eta) = \theta_m^*(\eta) + C_4e^{\eta} + C_5e^{-\eta}, \quad (47)$$

in which the f_m^* and θ_m^* indicate the special solutions.

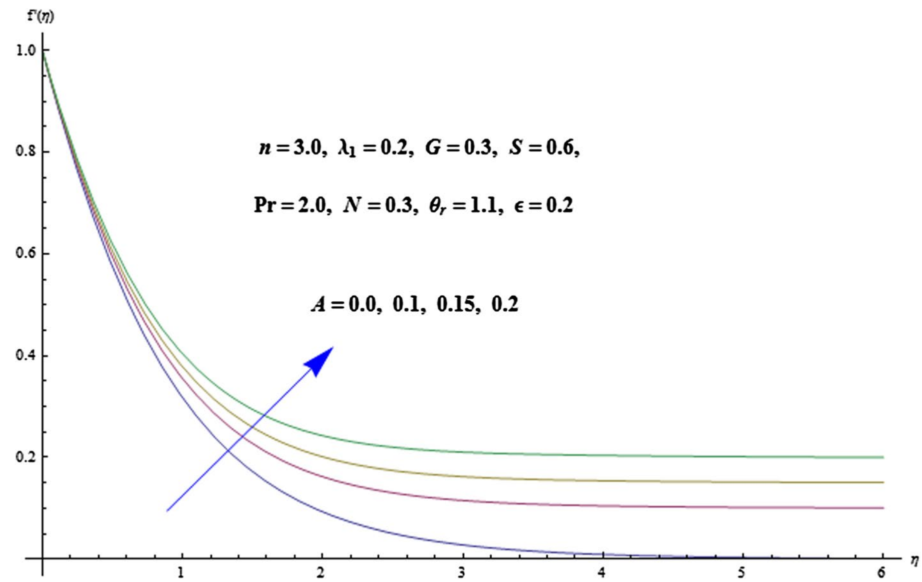

Fig. 2 Effects of A on $f'(\eta)$

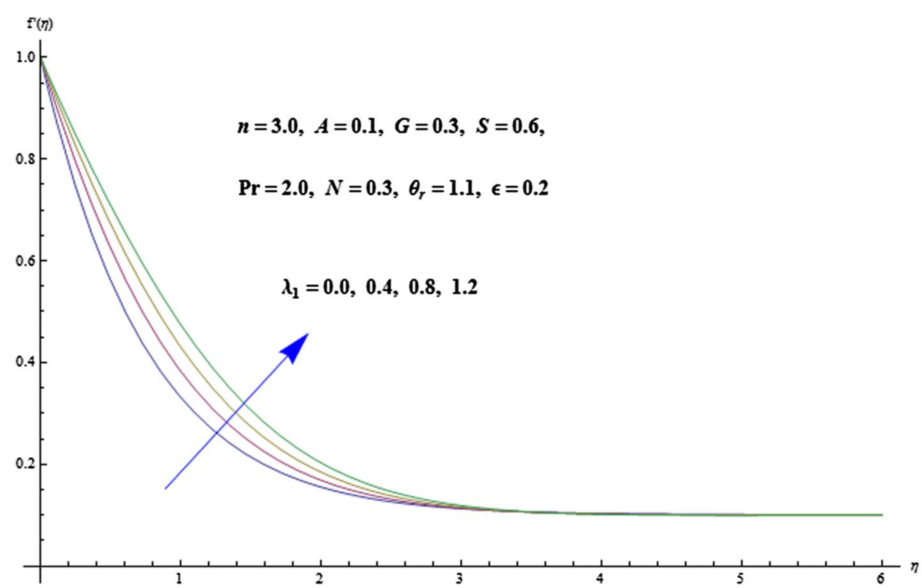

Fig. 3 Effects of λ_1 on $f'(\eta)$

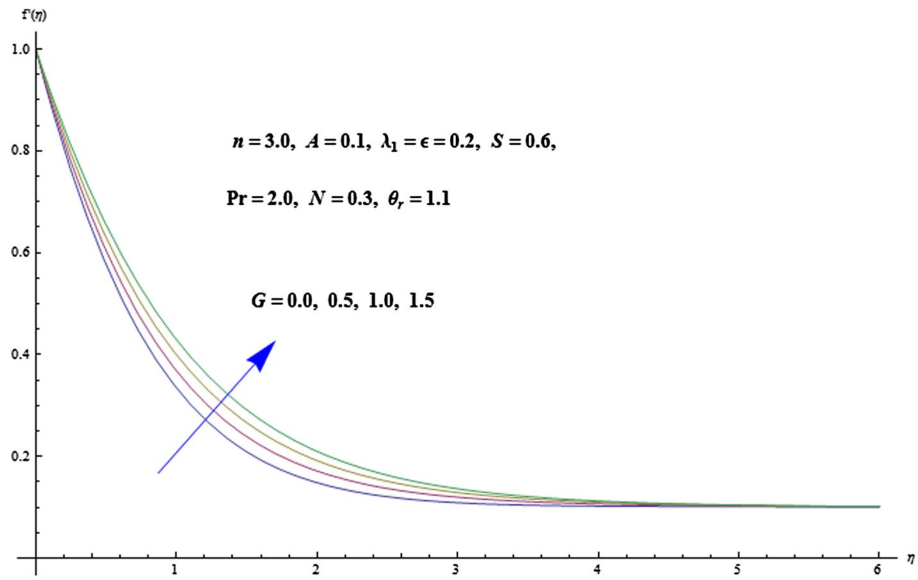

Fig. 4 Effects of G on $f'(\eta)$

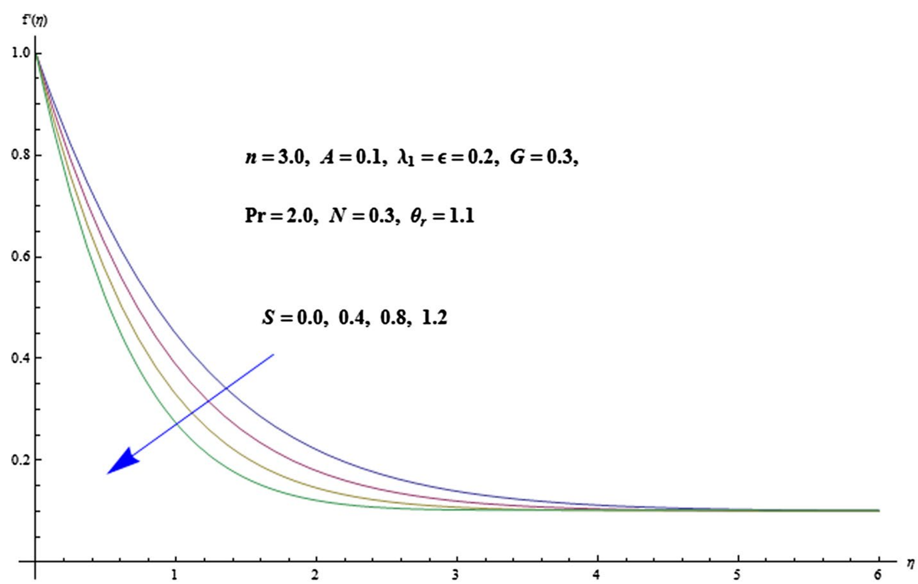

Fig. 5 Effects of S on $f'(\eta)$

4 Convergence of the homotopy solutions

Here, our desire is to ensure the convergence of the obtained series solutions. Thus Fig. 1 has been plotted for the admissible values of $\hbar_f$ and $\hbar_\theta$ regarding convergence of the solutions (39) and (40). Ultimate the admissible values have been noticed in the ranges $-1.30 \leq \hbar_f \leq -0.20$ and $-1.40 \leq \hbar_\theta \leq -0.30$.

5 Discussion

This section elaborates the influence of different parameters on velocity f' and temperature profile θ. Figures 2, 3, 4, 5, 6 and 7 show the variations of different parameters A, λ_1, G, S, n and θ_r on the velocity f'. The effects of A on the velocity f' are shown in Fig. 2. It is revealed that the velocity f' enhances for larger values of A. The thickness of boundary layer is stronger for $A < 1$. Here the stretching rate dominates over the free stream rate. For $A > 1$ (the stretching rate of velocity is lower than free stream velocity rate) the thickness of boundary layer reduces while the velocity f' enhances. For $A = 1$, no boundary layer situation appeared. Figure 3 explores the effect of material parameter λ_1 on f'. By increasing λ_1 the velocity enhances and the profiles approaches to zero as $\eta \rightarrow \infty$. This shows an enhancement in hydrodynamic boundary layer. It is pointed out that the values of Carreau number vary from 0.1 to 20. Figure 4 shows the influence of mixed convection parameter G on velocity f'. We can

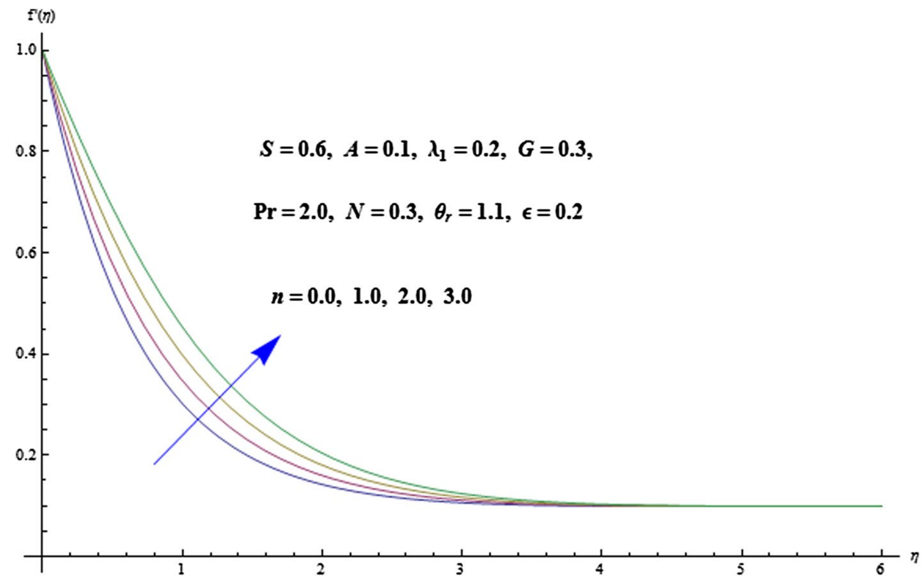

Fig. 6 Effects of n on $f'(\eta)$

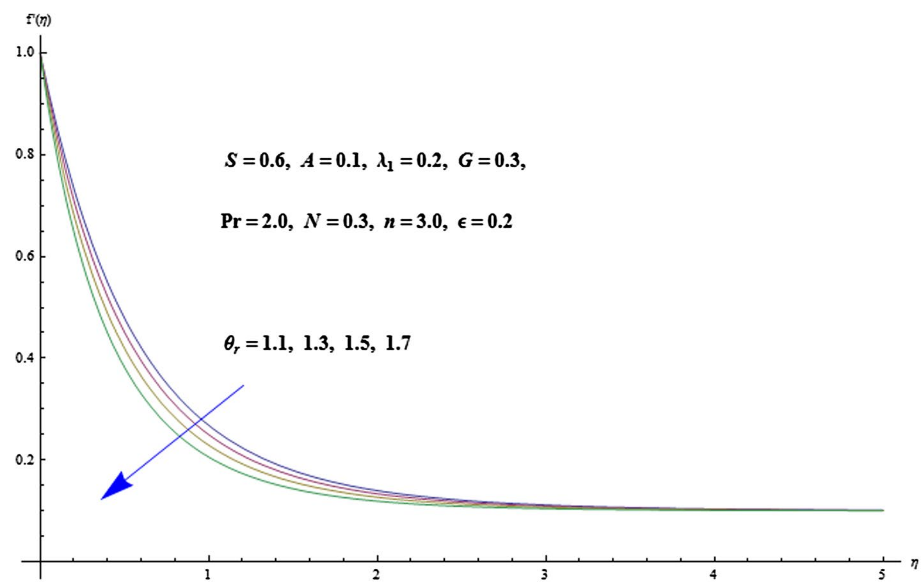

Fig. 7 Effects of $\theta_r > 0$ on $f'(\eta)$

see that velocity profile increases with an enhancement in the mixed convection parameter G. Physically, the buoyancy force takes place due to consideration of mixed convective parameter which enhances the velocity f'. The impacts of suction parameter S on velocity f' are visualized in Fig. 5. The liquid particles are sucked by sheet due to the larger suction parameter that offers a resistance to fluid flow and hence the velocity f' decreases. Figure 6 elucidates the variation of power law index n on velocity f'. The liquid velocity increases due to presence of power law index. The non-linearity of sheet is enhanced for larger n due to which the resistive force decreases and hence a reduction in velocity f' is achieved. Characteristics of θ_r on $f'(\eta)$ are addressed through Figs. 7 and 8. Here $f'(\eta)$ decays for $\theta_r > 0$ (i.e. for gases) whereas reverse behavior is noted for $\theta_r < 0$ (i.e. for liquids). Physically larger θ_r diminishes convective potential between the heated surface and ambient liquid and so $f'(\eta)$ decays.

Figures 9, 10, 11, 12, 13, 14 and 15 show the influence of different parameters A, S, Pr, N, ε and θ_r on temperature profile $\theta(\eta)$. The effects of A on temperature profile θ are shown in Fig. 9. We can see that the temperature profile decreases by increasing A. Higher values of A correspond to more pressure which provides less resistance to

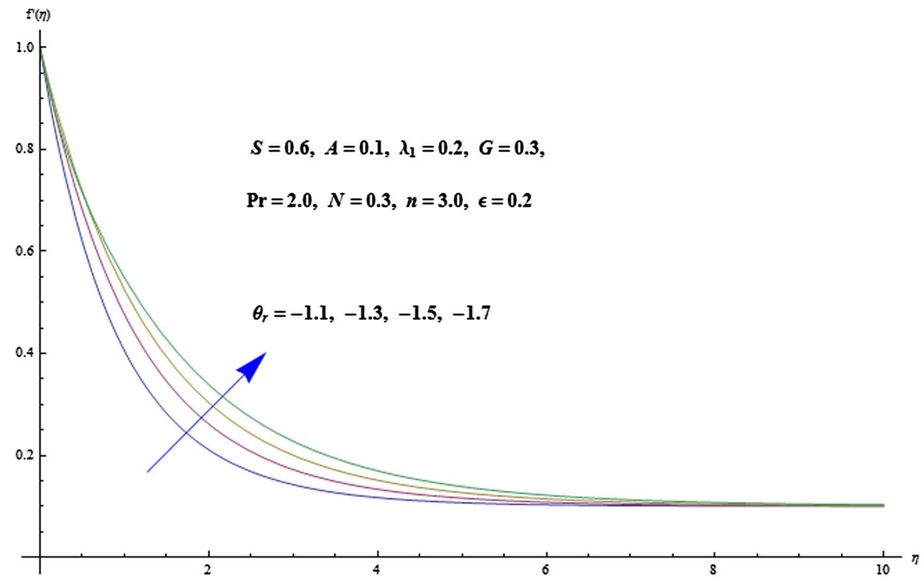

Fig. 8 Effects of $\theta_r < 0$ on $f'(\eta)$

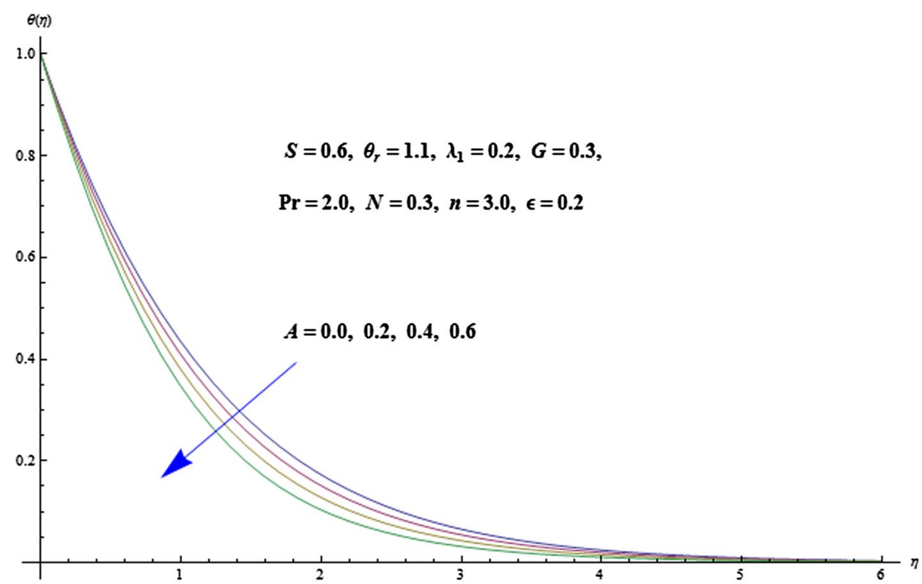

Fig. 9 Effects of A on $\theta(\eta)$

fluid. Hence less heat is produced and temperature profile reduces. Figure 10 shows the behavior of S on temperature profile. Clearly, temperature profile reduces for larger S. In fact some fluid particles are absorbed by the sheet and each particle has energy which is transferred to the environment. Therefore, temperature of the fluid decreases. The conduction phenomenon decreases while pure convection enhanced due to an increase in Prandtl number Pr. That fact leads to lower temperature and thickness of thermal boundary layer (see Fig. 11). Small values of the Prandtl number $\Pr \ll 1$ means the thermal diffusivity dominates whereas the large values $\Pr \gg 1$ implies the momentum diffusivity dominates the behavior. It depends on the fluid properties like for gases Pr ranges 0.7–1.0, for water Pr ranges 1–10, for liquid metals Pr ranges 0.001–0.03 and for oils Pr ranges 50–2000. Figure 12 explores the variations of N on temperature θ. Here, we revealed that the temperature and its related thickness of boundary layer are higher for larger N. Influence of ε on temperature profile is presented in Fig. 13 It is examined that large amount of heat transfers from surface to material and thus $\theta(\eta)$ increases. Figures 14 and 15 are disclosed to analyze the impacts of $\theta_r > 0$ and

Fig. 10 Effects of S on $\theta(\eta)$

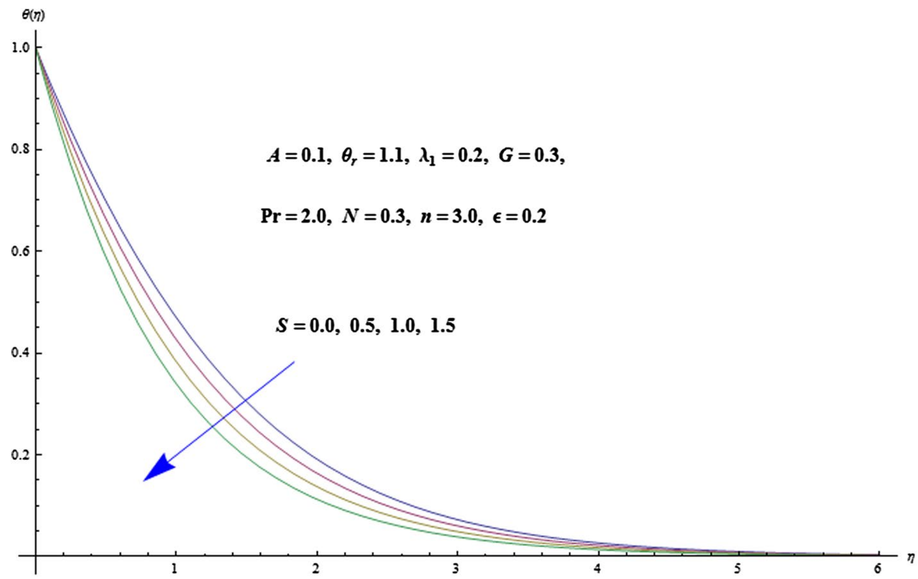

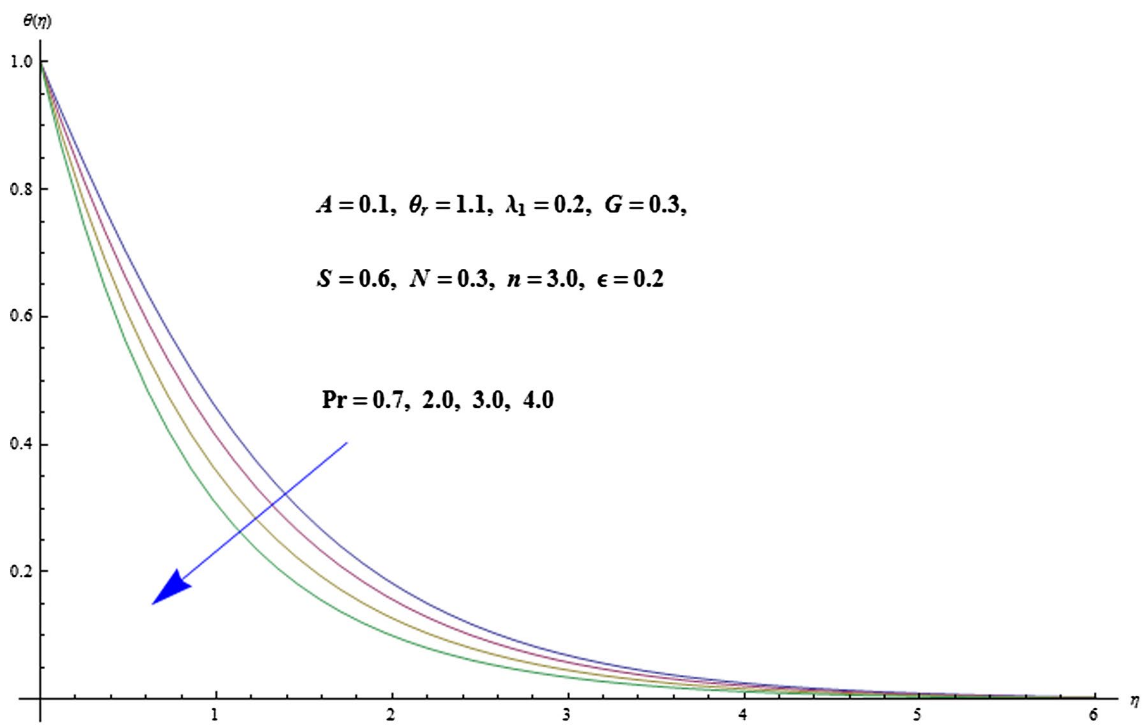

Fig. 11 Effects of Pr on $\theta(\eta)$

$\theta_r < 0$ on temperature $\theta(\eta)$. Clearly $\theta(\eta)$ boosts when $\theta_r > 0$. However, opposite situation is examined for $\theta_r < 0$.

Table 1 is presented to find that how much order of computations is required for a convergent solution. It is noticed that 15th and 20*th* order of deformations are required for the velocity and temperature solutions respectively. Table 2 is made to analyze the numerical values of skin friction coefficient and local Nusselt number for different values of A, G, S, θ_r, Pr and N. This Table elaborates that heat transfer rate become larger when we

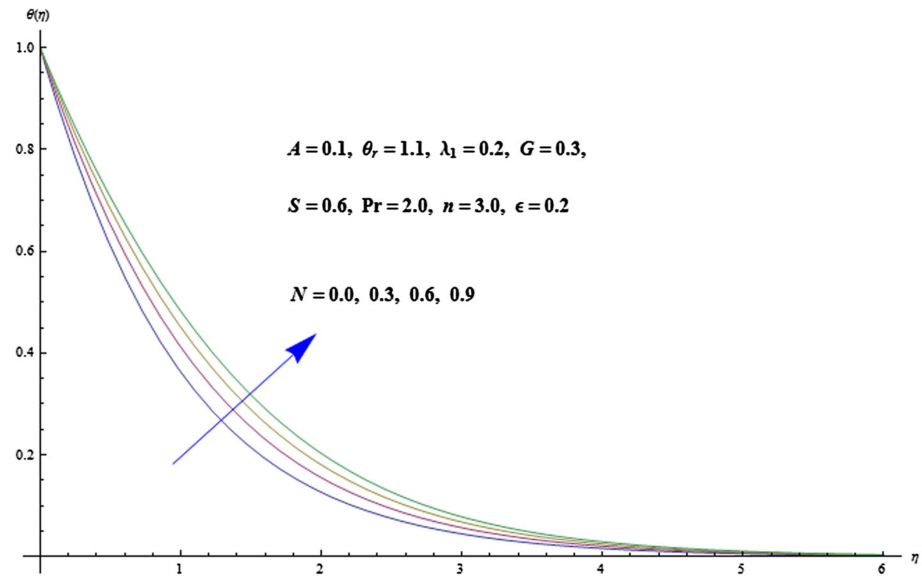

Fig. 12 Effects of N on $\theta(\eta)$

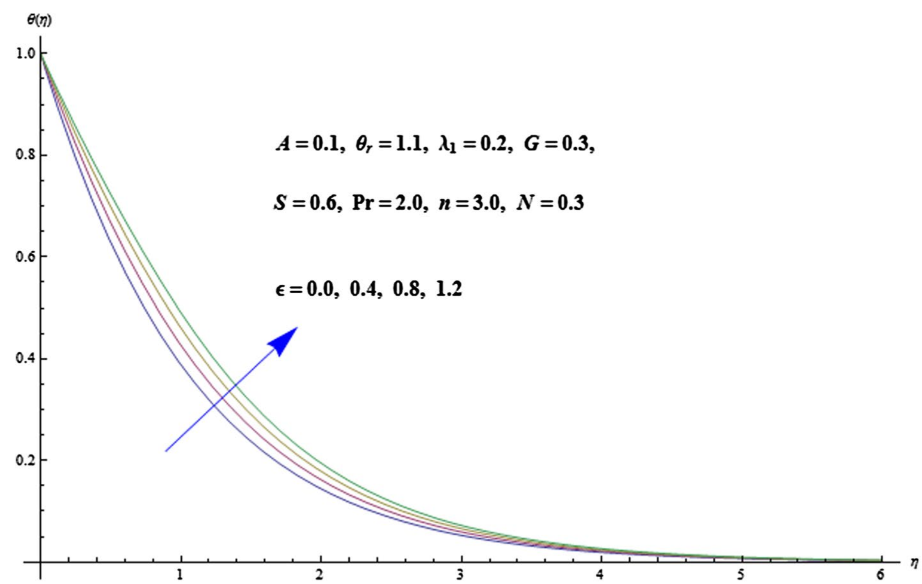

Fig. 13 Effects of ε on $\theta(\eta)$

increase the values of A, G, S, Pr and N; however, opposite situation is noticed for larger θ_r. Moreover, skin friction coefficient becomes larger when we increase Pr and S while it reduces via larger A, G, θ_r and N. Tables 3 and 4 provides a comparative analysis of existing solutions with the previous results in a limiting case. From these

Fig. 14 Effects of $\theta_r > 0$ on $\theta(\eta)$

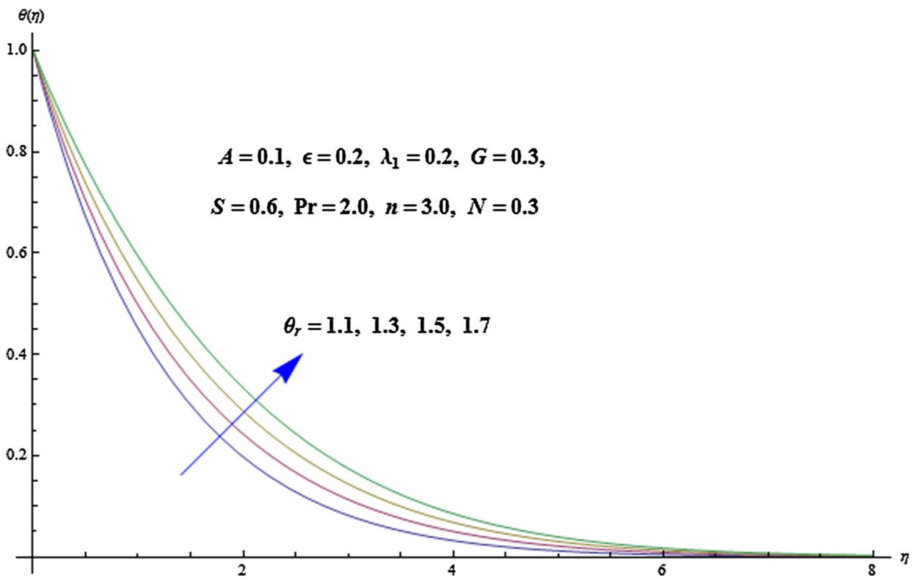

Fig. 15 Effects of $\theta_r < 0$ on $\theta(\eta)$

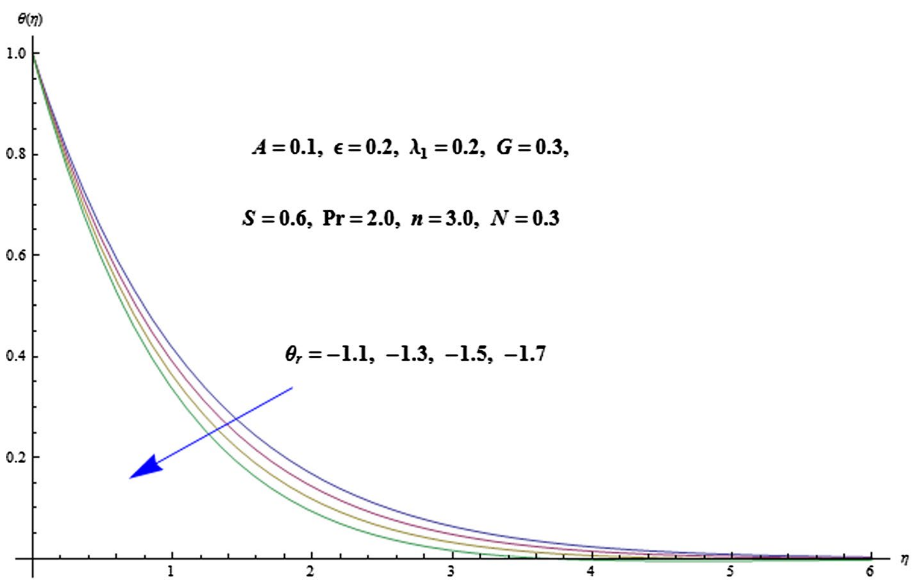

Table 1 Convergence of homotopy solutions when $n = 3$, $G = 0.3$, $\lambda_1 = \varepsilon = 0.2$, $A = 0.1$, $S = 0.6$, $\Pr = 2.0$, $\theta_r = 1.1$ and $N = 0.3$

Order of approximation	$-f''(0)$	$-\theta'(0)$
1	1.0001	0.32381
5	1.0199	0.31553
10	1.0182	0.31485
15	1.0182	0.31481
20	1.0182	0.31481
25	1.0182	0.31481
30	1.0182	0.31481
35	1.0182	0.31481

Tables, we have examined that our present solutions have an excellent match with the previous published data that shows the reliability and validity of technique used for the computations.

6 Concluding remarks

Mixed convective flow of Carreau liquid near a stagnation point considering variable properties is examined. The following conclusions can be extracted from this investigation:

Table 2 Numerical data of skin friction coefficient and local Nusselt number for various values of A, G, S, θ_r, Pr, and N when $\lambda_1 = 0.2$, $\varepsilon = 0.2$ and $n = 3.0$

A	G	S	θ_r	Pr	N	$C_f Re_x^{\frac{1}{2}}$	$Re_x^{-\frac{1}{2}} Nu_x$
0.0	0.3	0.5	1.1	2.0	0.6	−1.2607	0.4354
0.2						−1.1608	0.4458
0.4						−0.9798	0.4549
0.1	0.0					−1.2823	0.4386
	0.4					−1.2021	0.4414
	0.8					−1.1247	0.4438
	0.3	0.0				−0.9409	0.4067
		0.3				−1.0755	0.4238
		0.7				−1.2727	0.4463
		0.6	3.0			−1.8790	0.8917
			5.0			−1.6971	0.8874
			7.0			−1.6383	0.8856
			0.5	1.0		−1.2392	0.4810
				1.1		−1.2431	0.4913
				1.2		−1.2465	0.5004
				2.0	0.0	−1.2384	0.3420
					0.2	−1.2271	0.4092
					0.4	−1.2167	0.4710

Table 3 Comparison of present results of $f''(0)$ with [34] for different values of A when $n = 1.0$, and $S = 0.0 = \lambda_1 = G = \theta_r$

A	Ref. [34]	Present
0.01	−0.9963	−0.998024
0.02	−0.9930	−0.995783
0.05	−0.9830	−0.987580
0.10	−0.9603	−0.969386
0.20	0.9080	−0.918107
0.50	0.6605	−0.667260
1.00	0.0000	0.000000
2.00	2.0181	2.01767
3.00		4.72964

Table 4 Comparison of present results of $\theta'(0)$ with those of [35] when $N = \varepsilon = 0$

Pr	A	Ref. [35]	Present
1.0	0.1	0.602156	0.602156
	0.5	0.692460	0.692460
1.5	0.1	0.776802	0.776802
	0.5	0.864771	0.864771

- Impact of A on temperature and velocity fields is quite reverse. Velocity is increased while temperature reduces with an increase in A.
- Suction parameter S reduced the velocity of liquid while it increases the momentum boundary layer thickness.
- Prandtl number Pr creates a reduction in temperature $\theta(\eta)$ and thickness of thermal boundary layer.
- The increasing values of θ_r (i.e. $\theta_r > 0$) correspond to lower velocity and higher temperature.
- The effects of S and Pr on temperature $\theta(\eta)$ are similar in a qualitatively way.

References

1. Hsu JP, Hung SH, Yu H (2004) Electrophoresis of a sphere at an arbitrary position in a spherical cavity filled with Carreau fluid. J Colloid Interface Sci 280:256–263
2. Ali N, Hayat T (2007) Peristaltic motion of a Carreau fluid in an asymmetric channel. Appl Math Comput 193:535–552
3. Shamekhi A, Sadeghy K (2009) Cavity flow simulation of Carreau–Yasuda non-Newtonian fluids using PIM meshfree method. Appl Math Model 33:4131–4145
4. Tshehla MS (2011) The flow of Carreau fluid down an incline with a free surface. Int J Phys Sci 6:3896–3910
5. Olajuwon BI (2011) Convective heat and mass transfer in a hydromagnetic Carreau fluid past a vertical porous plated in presence of thermal radiation and thermal diffusion. Therm Sci 15:241–252
6. Hayat T, Asad S, Mustafa M, Alsaedi A (2014) Boundary layer flow of Carreau fluid over a convectively heated stretching sheet. Appl Math Comput 246:12–22
7. Raju CSK, Sandeep N (2016) Falkner-Skan flow of a magnetic-Carreau fluid past a wedge in the presence of cross diffusion effects. Eur Phys J Plus 131:267
8. Machireddy GR, Naramgari S (2016) Heat and mass transfer in radiative MHD Carreau fluid with cross diffusion. Ain Shams Eng J. doi:10.1016/j.asej.2016.06.012
9. Sulochana C, Ashwinkumar GP, Sandeep N (2016) Transpiration effect on stagnation-point flow of a Carreau nanofluid in

the presence of thermophoresis and Brownian motion. Alex Eng J 55:1151–1157
10. Raju CSK, Sandeep N (2016) Unsteady three-dimensional flow of Casson-Carreau fluids past a stretching surface. Alex Eng J 55:1115–1126
11. Hayat T, Waqas M, Shehzad SA, Alsaedi A (2016) Stretched flow of Carreau nanofluid with convective boundary condition. Pram J Phys 86:3–17
12. Hiemenz K (1911) Die Grenzschicht an einem in den gleichförmigen Flüssigkeitsstrom eingetauchten geraden Kreiszylinder. Int J Dingler's Polytech 326:321–324
13. Mahapatra TR, Gupta AS (2002) Heat transfer in stagnation-point flow towards a stretching sheet. Int J Heat Mass Transf 38:517–521
14. Nazar R, Amin N, Filip D, Pop I (2004) Stagnation-point flow of a micropolar fluid towards a stretching sheet. Int J Non-Linear Mech 39:1227–1235
15. Mustafa M, Hayat T, Pop I, Asgar S, Obaidat S (2012) Stagnation-point flow of a nanofluid towards a stretching sheet. Int J Heat Mass Transf 54:5588–5594
16. Alsaedi A, Awais M, Hayat T (2012) Effects of heat generation/absorption on stagnation point flow of nanofluid over a surface with convective boundary conditions. Commun Nonlinear Sci Numer Simul 17:4210–4223
17. Turkyilmazoglu M, Pop I (2013) Exact analytical solutions for the flow and heat transfer near the stagnation point on a stretching/shrinking sheet in a Jeffrey fluid. Int J Heat Mass Transf 57:82–88
18. Hayat T, Anwar MS, Farooq M, Alsaedi A (2014) MHD stagnation point flow of second grade fluid over a stretching cylinder with heat and mass transfer. Int J Nonlin Sci Numer Simul 15:365–376
19. Shehzad SA, Hayat T, Asghar S, Alsaedi A (2015) Stagnation point flow of thixotropic fluid with mass transfer and chemical reaction. J Appl Fluid Mech 8:465–471
20. Turkyilmazoglu M (2012) Solution of Thomas-Fermi equation with a convergent approach. Commun Nonlinear Sci Numer Simul 17:4097–4103
21. Rashidi MM, Rajvanshi SC, Keimanesh M (2012) Study of pulsatile flow in a porous annulus with the homotopy analysis method. Int J Numer Methods Heat Fluid Flow 22
22. Hassan HN, Rashidi MM (2014) An analytic solution of micropolar flow in a porous channel with mass injection using homotopy analysis method. Int J Numer Methods Heat Fluid Flow 24:419–437
23. Zheng L, Zheng C, Zheng X, Zhang J (2013) Flow and radiation heat transfer of a nanofluid over a stretching sheet with velocity slip and temperature jump in porous medium. J Franklin Inst 350:990–1007
24. Abbasbandy S, Hayat T, Alsaedi A, Rashidi MM (2014) Numerical and analytical solutions for Falkner-Skan flow of MHD Oldroyd-B fluid. Int J Numer Methods Heat Fluid Flow 24:390–401
25. Abbasbandy S, Hashemi MS, Hashim I (2013) On convergence of homotopy analysis method and its application to fractional integro-differential equations. Quaestiones Math 36:93–105
26. Hayat T, Shehzad SA, Al-Sulami HH, Asghar S (2013) Influence of thermal stratification on the radiative flow of Maxwell fluid. J Br Soc Mech Sci Eng 35:381–389
27. Abbasi FM, Shehzad SA, Hayat T, Alsaedi A, Obid MA (2015) Influence of heat and mass flux conditions in hydromagnetic flow of Jeffrey nanofluid. AIP Adv 5:037111
28. Hayat T, Khan MI, Farooq M, Yasmeen T, Alsaedi A (2016) Stagnation point flow with Cattaneo–Christov heat flux and homogeneous-heterogeneous reactions. J Mol Liq 220:49–55
29. Shehzad SA, Hayat T, Alsaedi A, Chen B (2016) A useful model for solar radiation. Energy Ecol Environ 1:30–38
30. Hayat T, Waqas M, Shehzad SA, Alsaedi A (2016) On 2D stratified flow of an Oldroyd-B fluid with chemical reaction: an application of non-Fourier heat flux theory. J Mol Liq 223:566–571
31. Tsai R, Huang KH, Huang JS (2009) The effects of variable viscosity and thermal conductivity on heat transfer for hydromagnetic flow over a continuous moving porous plate with Ohmic heating. Appl Thermal Eng 29:1921–1926
32. Magyari E, Pantokratoras A (2011) Note on the effect of thermal radiation in the linearized Rosseland approximation on the heat transfer characteristics of various boundary layer flows. Int Commun Heat Mass Transf 38:554–556
33. Haq RU, Nadeem S, Akbar NS, Khan ZH (2015) Buoyancy and radiation effect on stagnation point flow of micropolar nanofluid along a vertically convective stretching surface. IEEE Trans Nanotechnol 14:42–50
34. Hayat T, Hussain Z, Farooq M, Alsaedi A, Obaid M (2014) Thermally stratified stagnation point flow of an Oldroyd-B fluid. Int J Nonlinear Sci Numer Simul 15:77–86
35. Awais M, Hayat T, Alsaedi A (2015) Investigation of heat transfer in flow of Burgers' fluid during a melting process. J Egypt Soc 23:410–415